PROCEEDINGS A

royalsocietypublishing.org/journal/rspa

CC BY

Research

Cite this article: Crowdy DG. 2024 Torque-driven superhydrophobic cylinders swim in circles. *Proc. R. Soc. A* **480**: 20240149.
https://doi.org/10.1098/rspa.2024.0149

Received: 25 February 2024
Accepted: 23 August 2024

Subject Category:
Mathematics

Subject Areas:
applied mathematics, mathematical modelling, mechanical engineering

Keywords:
superhydrophobicity, Stokes flow, complex analysis

Author for correspondence:
Darren G. Crowdy
e-mail: d.crowdy@imperial.ac.uk

Downloaded from https://royalsocietypublishing.org/ on 28 October 2024

Torque-driven superhydrophobic cylinders swim in circles

Darren G. Crowdy

Department of Mathematics, Imperial College London, 180 Queen's Gate, London SW7 2AZ, UK

DGC, 0000-0002-7162-0181

A superhydrophobic cylinder is a circular cylinder with a boundary pattern of alternating shear-free menisci and solid portions. This article derives analytical solutions for the torque-driven Stokes flow around a superhydrophobic cylinder that is free to move, or 'swim', subject to the constraint that it is free of net force. The mathematical approach is a natural generalization of one used to solve for transverse shear flow over a superhydrophobic surface comprising a periodic array of no-shear slots (Crowdy 2011 *Phys. Fluids* **23** (doi:10.1063/1.3605575)). First, the torque-driven Stokes flow around a superhydrophobic cylinder with two unequal no-shear menisci and two equal solid portions is solved in detail. It is then shown how that analysis generalizes, in a natural way, to a cylinder with M no-shear menisci between M solid portions with full exposition given of the case of $M = 3$ equal solid portions. A further generalization to flow around a superhydrophobic cylinder with an N-fold rotationally symmetric patterning with M menisci in each $2\pi/N$ sector is made. Torque-driven superhydrophobic cylinders with a no-shear pattern devoid of any rotational symmetry are shown to swim on circular trajectories with formulas for the radius and cylinder angular velocity on these trajectories derived here as functions of the no-shear pattern geometry. The $M = 1$ case of a 'Janus' superhydrophobic cylinder having one meniscus and one solid portion can be solved completely explicitly.

© 2024 The Author(s). Published by the Royal Society under the terms of the Creative Commons Attribution License http://creativecommons.org/licenses/by/4.0/, which permits unrestricted use, provided the original author and source are credited.

THE ROYAL SOCIETY PUBLISHING

royalsocietypublishing.org/journal/rspa Proc. R. Soc. A 480: 20240149

Downloaded from https://royalsocietypublishing.org/ on 28 October 2024

1. Introduction

The study of superhydrophobicity is a highly active area of research. Surface roughness leads to trapped regions of air, in a so-called Cassie state, with the drag on flow over such surfaces generally reduced because of decreased contact with no-slip regions that have been replaced by shear-free surfaces.

Ou & Rothstein [1] performed an early experimental study to demonstrate that superhydrophobic surfaces can reduce drag in laminar channel flows. A few years later, Rothstein [2] reviewed the intense activity in the area, including work on the theoretical quantification of the slipperiness of such surfaces. The effect of adding no-shear stripes to finite objects has also been studied, including experimental work investigating the effect on vortex shedding in flow past superhydrophobic cylinders [3]. How the Stokes drag on a finite object is affected when it is situated near a planar superhydrophobic surface has also been investigated [4].

Lauga & Stone [5] studied the effective slip length of a surface patterned with no-shear regions, a useful diagnostic quantifying the degree to which a given surface diverges from being no-slip. They made use of a much earlier study by Philip [6], who used complex analysis techniques to study a range of mixed boundary value problems comprising flow over combinations of no-slip and no-shear surfaces. These boundary value problems, which are characterized by a mix of Dirichlet- and Neumann-type boundary conditions and are canonical in many physical applications (e.g. [7,8]), include shear flow over a flat surface with a periodic array of no-shear slots, and pressure-driven flow in channels and pipes with similar no-shear patterning. Philip's analytical solutions have since been generalized in a number of directions [9–13]. Of particular relevance to the present article is the generalization by the author [9], who used complex analysis and the theory of prime functions [14] to generalize Philip's solution for shear flow over a periodic array of no-shear slots to the case where there is still a periodic array of no-shear slots but with more than one slot in each period window.

Yariv & Siegel [15] and Siegel & Yariv [16] recently studied Stokes flow around a fixed superhydrophobic cylinder subject to an external torque. A superhydrophobic cylinder is a two-dimensional object having a circular boundary with a surface pattern of no-shear slots alternating with no-slip regions. This problem can be viewed as a radial geometry analogue of the periodic problem of transverse shear flow over no-shear slots studied by Philip [6] and reappraised in Crowdy [9]. The key result of Yariv & Siegel [15], which studied the case of an N-fold rotationally symmetric distribution of no-shear slots, was to derive the following mobility relation

$$1+\frac{2}{N}\log\operatorname{cosec}\left(\frac{\pi\phi}{2}\right), \tag{1.1}$$

quantifying the enhancement in the angular velocity of a superhydrophobic cylinder, in response to the external torque, as a function of the solid fraction ϕ. They proved that (1.1) holds for $N = 1,2,4,8,\ldots$ and conjectured that it furnishes the result for all $N \geq 1$. Siegel & Yariv [16] later studied the problem numerically, using a complex analysis reformulation as a Hilbert problem, and confirmed that formula (1.1) agrees to high precision with the numerical results for any $N \geq 1$. Their numerical method allowed for no-shear slot arrangements without any rotational symmetries and they observed that, in such cases, a non-zero uniform flow, referred to as a 'streaming flow', is generally observed in the far-field and this phenomenon was discussed in the context of Jeffery's paradox.

The present article has been motivated by the recent work in Yariv & Siegel [15] and Siegel & Yariv [16] but adopts a different view of the problem, one more relevant to a growing literature on torque-driven active matter, including the study of fluid manipulation in microdevices using rotating cylindrical micro-pumps or rotors. External magnetic fields can be used, for example to directly manipulate individual colloidal particles by applying a torque to them, which can be converted to translational motion via a number of strategies. At very

Downloaded from https://royalsocietypublishing.org/ on 28 October 2024

low Reynolds numbers, some means of breaking the inherent time-reversal symmetry in such flows [17] must occur: a recent review by Driscoll & Delmotte [18] surveys a number of these, including adding flagella or cilia to particles, or rotating the particles by an external magnetic field near a solid surface. Another strategy is to rotate them near a free surface and this has other implications reviewed by Snezhko [19]. The interaction of self-actuated 'micro-rotors', or swimmers that exert a net torque on the fluid and interact via hydrodynamic interactions, has been studied by Lushi & Vlahovska [20], who found periodic and chaotic dynamics. It is also known that the motion of large numbers of torque-driven particles or 'micro-rollers' near a wall leads to interesting collective behaviour [21,22]. A recent review with a focus on torque-driven particles has been provided by Martinez-Pedrero & Tierno [23]. Propulsion in viscous fluids is important across a wide range of areas, including targeted drug delivery, microsurgery, the study of biological microorganisms [24] and particle transport in microfluidic systems [25].

The present article reconsiders Stokes flow around a superhydrophobic cylinder, with geometry akin to that considered in Yariv & Siegel and Siegel & Yariv [15,16], but where such a cylinder is not fixed in place but is free to move in response to an external torque and subject to the constraint that it is free of net force. The superhydrophobic cylinder is therefore viewed here as a type of externally driven, low-Reynolds-number swimmer. Since the problem is two-dimensional, the Stokes paradox [26,27] requires the constraint of zero net force on the cylinder in order for a solution to exist. The physical mechanism supplying the external torque is not discussed; rather, interest here is in how patterning a cylindrical particle with no-shear stripes can provide a source of translational–rotational coupling so that an imposed torque can lead to a translational velocity, that is, a swimming superhydrophobic cylinder. This article will show that superhydrophobic cylinders devoid of any rotational symmetry swim in circular trajectories with the radius of those trajectories, and cylinder speed on them, determinable from the geometry of the no-shear patterning using the analytical tools set out here. The solution for a superhydrophobic cylinder with a single no-shear meniscus is shown to be solvable in a completely explicit form.

Another way to view the problem is in terms of a mobility matrix. Let (U_c, V_c) denote the translational velocity of the superhydrophobic cylinder in Cartesian (x, y) coordinates and let Ω denote its angular velocity about its centre. If these quantities are collected in the vector $\mathbf{U} = (U_c, V_c, \Omega)$, then the mobility matrix components $\mathbf{M}_{ij}$ are such that:

$$\mathbf{U}_i = \mathbf{M}_{ij}\mathbf{F}_j, \tag{1.2}$$

where the vector $\mathbf{F} = (F_x, F_y, T)$ contains the external forces (F_x, F_y) in the x and y directions and the external torque T applied to the cylinder. Because of the Stokes paradox [26,27], the first two columns of the mobility matrix do not exist. The only well-defined components for a superhydrophobic cylinder are $\{\mathbf{M}_{i3}\}$, the third column of the mobility matrix, namely, those components that determine the cylinder velocity and angular velocity in response to just an external torque T. These quantities will be determined in this article. A by-product is to retrieve some results of Yariv & Siegel [15] and Siegel & Yariv [16] using a novel approach, and in an alternative explicit form not requiring integrals. Indeed, it is shown here that the problems of torque-driven Stokes flow around a swimming superhydrophobic cylinder can be solved by a direct extension of the conformal mapping methods—based on prime functions and certain conformal slit mappings built from them—that was introduced for flows over periodic superhydrophobic surfaces in Crowdy [9,28]. And, just as the mixed boundary value problems solved by Philip [6] are canonical in the sense of being relevant to many applications, the mixed boundary value problems solved here are similarly likely to find use in other contexts.

Downloaded from https://royalsocietypublishing.org/ on 28 October 2024

2. Complex variable formulation

Since the superhydrophobic cylinder, of radius a, to be considered is allowed to move it is appropriate to solve for the quasi-steady Stokes flow around it in a body-fixed (x, y) frame of reference with origin taken at its centre. With the introduction of the complex variable $z = x + \mathrm{i}y$ in this frame, the cylinder boundary corresponds to $|z| = a$ and the fluid of viscosity μ occupies $|z| > a$. Ignoring inertia in the fluid exterior to the cylinder, its velocity $\mathbf{u} = (u, v)$ satisfies the quasi-steady incompressible Stokes equations

$$\mu \nabla^2 \mathbf{u} = \nabla p, \qquad \nabla . \mathbf{u} = 0, \tag{2.1}$$

where p is the pressure in the fluid. On taking the curl of (2.1) it is well-known [29] that such a two-dimensional flow is describable by a biharmonic streamfunction $\psi(z, \bar{z})$ associated with flow $\mathbf{u} = (u, v)$ given by

$$\psi(z, \bar{z}) = \mathrm{Im}[\bar{z} f(z) + g(z)], \qquad (u, v) = \left(\frac{\partial \psi}{\partial y}, -\frac{\partial \psi}{\partial x} \right), \tag{2.2}$$

where $f(z)$ and $g(z)$ are two (Goursat) functions of $z = x + \mathrm{i}y$ analytic for $|z| > a$ but with possible singularities at infinity. It can be shown [29] that the fluid pressure p, the vorticity $\omega = -\nabla^2 \psi$ and the fluid rate-of-strain tensor $e_{ij} = (1/2)(\partial u_i / \partial x_j + \partial u_j / \partial x_i)$ are related to $f(z)$ and $g(z)$ through:

$$\begin{aligned} 4f'(z) &= \frac{p}{\mu} - \mathrm{i}\omega, \qquad u - \mathrm{i}v = -\overline{f(z)} + \bar{z} f'(z) + g'(z), \\ e_{11} + \mathrm{i}e_{12} &= z\overline{f''(z)} + \overline{g''(z)}, \end{aligned} \tag{2.3}$$

where the prime notation denotes differentiation with respect to z. The complex form of the fluid stress on the boundary, i.e. $-pn_i + 2\mu e_{ij} n_j$, is:

$$-2\mu \mathrm{i} \frac{dH}{ds}, \qquad H(z, \bar{z}) = f(z) + z\overline{f'(z)} + \overline{g'(z)}, \tag{2.4}$$

where the arclength s along the circular boundary increases in a clockwise direction. A fuller derivation of this complex variable formulation of two-dimensional quasi-steady Stokes flow can be found in an appendix of Crowdy [29]. At zero Reynolds number, the hydrodynamic torque on the cylinder must balance the external torque so that there is no net torque on it.

3. Torque on a solid cylinder

Before considering a superhydrophobic cylinder it is instructive to use the complex variable formulation to determine the steady flow around a solid cylinder of radius a experiencing a non-zero external torque, a problem that can be solved in various alternative ways [26,27]. This preliminary calculation also provides insight into how $g(z)$ must admit a logarithmic singularity in such a case.

From the rotational symmetry of this problem, the cylinder is not expected to displace but simply to rotate. The steady flow exterior to a no-slip cylinder rotating with angular velocity Ω_0 is

$$u - \mathrm{i}v = -\frac{\mathrm{i}\Gamma}{2\pi z}, \qquad \Gamma = 2\pi a^2 \Omega_0, \tag{3.1}$$

corresponding to

$$f(z) = 0, \qquad g(z) = -\frac{\mathrm{i}\Gamma}{2\pi} \log z, \tag{3.2}$$

Downloaded from https://royalsocietypublishing.org/ on 28 October 2024

as readily verified using (2.3). Introducing the usual analogues in the complex number field $\mathbb{C}$ of two vectors $\mathbf{a} = (a_x, a_y)$ and $\mathbf{b} = (b_x, b_y)$ in $\mathbb{R}^2$, namely $a = a_x + ia_y$ and $b = b_x + ib_y$, then the complex analogue of the out-of-plane component of $\mathbf{a} \wedge \mathbf{b}$ is $\mathrm{Im}[\bar{a}b]$ and the complex analogue of $\mathbf{a}.\mathbf{b}$ is $\mathrm{Re}[\bar{a}b] = \mathrm{Re}[a\bar{b}]$. The hydrodynamic torque T_0 on the solid cylinder is therefore:

$$T_0 = -\mathrm{Im}\left[\oint_{|z|=a} \bar{z}\left(-2\mu i\frac{dH}{ds}\right)ds\right], \tag{3.3}$$

where, on use of (3.2) in the definition of $H(z, \bar{z})$ given in (2.4),

$$H(z, \bar{z}) = \frac{i\Gamma}{2\pi\bar{z}}. \tag{3.4}$$

Therefore,

$$T_0 = -\mathrm{Im}\left[\oint_{|z|=a} \bar{z}\left(-2\mu i d\left(\frac{i\Gamma}{2\pi\bar{z}}\right)\right)\right] = \frac{\mu\Gamma}{\pi}\mathrm{Im}\left[\oint_{|z|=a}\frac{d\bar{z}}{\bar{z}}\right] = -4\pi\mu\Omega_0 a^2, \tag{3.5}$$

where the expression for Γ in (3.1) has been used as well as the fact that:

$$\oint_{|z|=a}\frac{dz}{z} = 2\pi i. \tag{3.6}$$

In view of this calculation, the Goursat functions (3.2) can now be rewritten as:

$$f(z) = 0, \qquad g'(z) = -\frac{i(-T_0)}{4\pi\mu z}, \tag{3.7}$$

where $-T_0$ is the external torque on the cylinder.

4. Torque on a superhydrophobic cylinder with $M = 2$ menisci

Using M to denote the number of no-shear menisci consider now a circular cylinder with $M = 2$ no-shear slots separated by two solid no-slip boundary portions as shown in figure 1. Attention is restricted to a cylinder where the two no-slip boundary portions have the same circumferential length, but the following analysis is easily extended if this restriction is relaxed. An important point is that the two menisci generally have different circumferential lengths so that such a superhydrophobic cylinder is not captured by the previous work of Yariv & Siegel [15] and Siegel & Yariv [16]. The special case where the two menisci happen to have equal lengths is captured, however, so too is the limiting case where one of the menisci vanishes, this being the single meniscus case. The following generalized analysis will be checked against previous work in those two special cases.

As in §3, a non-zero external torque T is applied to this superhydrophobic cylinder, but no external force. For general surface patterning without any symmetries, there is no reason to suppose *a priori* that the cylinder might not need to move, with speed (U_c, V_c) say, in order be free of net force. In the body-fixed frame moving with this (unknown) particle velocity, the far-field velocity will be irrotational and such that

$$u + iv \to -(U_c + iV_c), \qquad \text{as } |z| \to \infty. \tag{4.1}$$

While the cylinder does not translate in this body-fixed frame, it can nevertheless rotate with angular velocity Ω due to the external torque T. Since the flow is quasi-steady it can be assumed, without loss of generality, that the centre of one of the menisci is located instantaneously on the positive real axis. The aim is to find (U_c, V_c) and Ω in terms of T.

The dimensional Goursat functions encoding the Stokes flow will be taken to be

Downloaded from https://royalsocietypublishing.org/ on 28 October 2024

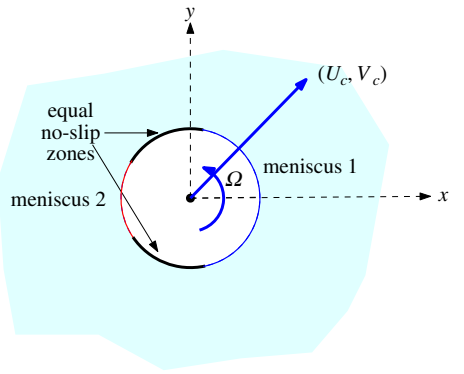


Figure 1. Superhydrophobic cylinder with two equal-length no-slip zones and $M = 2$ (generally unequal) menisci. An external torque T acts on the particle about its centre but there are no external forces. The aim is to find the induced Stokes flow, as well as the velocity (U_c, V_c) and angular velocity Ω of the cylinder, such that the net force and torque on it is zero.

$$f(z), \qquad g(z) = -\frac{\mathrm{i}T}{4\pi\mu}\log z - \frac{f(z)}{z}, \tag{4.2}$$

where the retention of the logarithmic singularity of $g(z)$ is motivated by the preliminary calculation in §3. This form also satisfies the condition that the boundary is a streamline as can be verified on substitution of (4.2) into (2.2); note that the cylinder boundary must be a streamline in the co-moving frame of reference. The function $f(z)$ must be single-valued and analytic in $|z| > a$ except for a simple pole at infinity where

$$f(z) \sim \frac{p_\infty}{4\mu} z + f_\infty + \mathcal{O}(1/z), \tag{4.3}$$

where the real constant p_∞ denotes the fluid pressure at infinity and $f_\infty \in \mathbb{C}$ is a complex constant that will be related shortly to the cylinder velocity (U_c, V_c). The single-valuedness of $f(z)$—and then also $g'(z)$, as follows from (4.2)—ensures that there is no net force on the cylinder as can be seen by integration of the boundary fluid stress (2.4) around the cylinder boundary while bearing in mind that $f(z)$ and $g'(z)$ must be such that $u + \mathrm{i}v$ as given by (2.3) is necessarily single-valued in the fluid region.

Both $f(z)$ and $g'(z)$ have the dimensions of velocity. Using hatted variables to denote non-dimensional counterparts, the mathematical problem will be non-dimensionalized as follows:

$$T = (-T_0)\hat{T}, \qquad z = a\hat{z}, \qquad s = a\hat{s}, \qquad (u, v) = a\Omega_0(\hat{u}, \hat{v}), \qquad f = a\Omega_0\hat{f}, \qquad g' = a\Omega_0\hat{g}'. \tag{4.4}$$

Henceforth, all hats will be dropped. Since arclength s increases in a clockwise direction, a parametrization of the cylinder boundary is provided by $z = e^{-\mathrm{i}s}$, from which it follows that the complex version of the unit tangent $\mathbf{t}$ is dz/ds and the complex version of the unit normal vector $\mathbf{n}$ pointing into the fluid are, respectively,

$$\frac{dz}{ds} = -\mathrm{i}z \qquad \mathrm{i}\frac{dz}{ds} = z. \tag{4.5}$$

It is also useful to note that, by the chain rule, on the cylinder boundary,

$$\frac{d}{ds} = \frac{dz}{ds}\frac{d}{dz} = -\mathrm{i}z\frac{d}{dz}. \tag{4.6}$$

Downloaded from https://royalsocietypublishing.org/ on 28 October 2024

(a) A mixed boundary value problem

It is necessary to formulate the boundary conditions on the solid portions and the menisci as conditions on the Goursat functions. Consider first the solid boundary portions. On differentiation of (4.2),

$$g'(z) = -\frac{\mathrm{i}T}{z} - \frac{f'(z)}{z} + \frac{f(z)}{z^2}. \tag{4.7}$$

The complex conjugate velocity field is then given by:

$$u - \mathrm{i}v = -\overline{f(z)} + \bar{z}f'(z) + g'(z) = -\overline{f(z)} + \bar{z}f'(z) - \frac{f'(z)}{z} + \frac{f(z)}{z^2} - \frac{\mathrm{i}T}{z}. \tag{4.8}$$

As $|z| \to \infty$, it follows from (4.1) and (4.8) that:

$$-(U_c - \mathrm{i}V_c) = -\overline{f_\infty}, \qquad \text{or} \qquad f_\infty = U_c + \mathrm{i}V_c, \tag{4.9}$$

where (4.3) has been used. On the cylinder boundary, $|z| = 1$ where $\bar{z} = 1/z$, (4.8) reduces to:

$$u - \mathrm{i}v = -\overline{f(z)} + \frac{f(z)}{z^2} - \frac{\mathrm{i}T}{z}. \tag{4.10}$$

If $U(s)$ is used to denote the tangential slip velocity then,

$$\begin{aligned} U(s) = \mathbf{u}\,.\,\mathbf{t} &= \mathrm{Re}\,[(u - \mathrm{i}v)(-\mathrm{i}z)] = \mathrm{Re}\left[\left(-\overline{f(z)} + \frac{f(z)}{z^2} - \frac{\mathrm{i}T}{z}\right)(-\mathrm{i}z)\right] \\ &= \mathrm{Re}\left[-\mathrm{i}\left(\frac{f(z)}{z} - \overline{\left(\frac{f(z)}{z}\right)}\right)\right] - T = \mathrm{Im}\left[\frac{2f(z)}{z}\right] - T\,. \end{aligned} \tag{4.11}$$

On the solid portions of the particle, it is necessary that:

$$U(s) = -\Omega, \tag{4.12}$$

where Ω is the angular velocity of the particle in the anticlockwise direction. Hence, on the solid portions of the particle boundary, it follows from (4.11) that:

$$\mathrm{Im}\left[\frac{2f(z)}{z}\right] = T - \Omega\,. \tag{4.13}$$

This condition suggests introducing the function:

$$h(z) \equiv \frac{2f(z)}{z}, \tag{4.14}$$

which is analytic and single-valued in $|z| > 1$, including at infinity as is evident from (4.3), which implies that, as $|z| \to \infty$,

$$h(z) \sim \frac{p_\infty}{2\mu} + \frac{2(U_c + \mathrm{i}V_c)}{z} + \mathcal{O}(1/z^2), \tag{4.15}$$

where (4.9) has also been used. The boundary condition (4.13) is:

$$\mathrm{Im}\,[h(z)] = T - \Omega\,. \tag{4.16}$$

The menisci, on the other hand, are free of shear stress, which, from (2.4), is equivalent to:

$$\mathrm{Re}\left[(\mathrm{i}\bar{z})\left(-2\mathrm{i}\frac{dH}{ds}\right)\right] = 0. \tag{4.17}$$

Equivalently, since $\bar{z} = 1/z$ on the menisci, this condition is:

$$\mathrm{Re}\left[\frac{1}{z}\frac{dH}{ds}\right] = \mathrm{Re}\left[\frac{1}{z}(-\mathrm{i}z)\frac{dH}{dz}\right] = 0, \qquad \text{or} \qquad \mathrm{Im}\left[\frac{dH}{dz}\right] = 0, \tag{4.18}$$

Downloaded from https://royalsocietypublishing.org/ on 28 October 2024

where (4.6) has been used. Since, on use of (4.7),

$$H(z,\overline{z}) = f(z) + z\overline{f'(z)} + \frac{\mathrm{i}T}{\overline{z}} - \overline{\left(\frac{f'(z)}{z}\right)} + \overline{\frac{f(z)}{z^2}}, \tag{4.19}$$

then, on $|z| = 1$

$$\frac{H(z,\overline{z})}{z} = \mathrm{Re}\left[\frac{2f(z)}{z}\right] + \mathrm{i}T\,. \tag{4.20}$$

It follows that:

$$H(z,\overline{z}) = z\mathrm{Re}\,[h(z)] + \mathrm{i}Tz, \tag{4.21}$$

implying, on differentiation with respect to z, that:

$$\frac{dH}{dz} = \mathrm{Re}[h(z)] + z\frac{d}{dz}\mathrm{Re}[h(z)] + \mathrm{i}T = \mathrm{Re}[h(z)] + \mathrm{i}\frac{d}{ds}\mathrm{Re}[h(z)] + \mathrm{i}T, \tag{4.22}$$

where (4.6) has been used again. On use of this relation, condition (4.18) becomes:

$$\mathrm{Im}\left[\frac{dH}{dz}\right] = \mathrm{Im}\left[\mathrm{i}\frac{d}{ds}\mathrm{Re}\,[h(z)] + \mathrm{i}T\right] = \frac{d}{ds}\mathrm{Re}\,[h(z)] + T = 0. \tag{4.23}$$

This can be integrated with respect to s on the i-th meniscus to give:

$$\mathrm{Re}[h(z)] = -Ts + c_i, \tag{4.24}$$

where c_i is a constant of integration specific to each meniscus. Without loss of generality, the choice $c_1 = 0$ can be made. From (4.14), and in view of (4.3), this sets a pressure level for the flow. The values of any other such constants are expected to be determined by the solution.

In summary, to solve the problem shown in figure 1, the challenge is to find a function $h(z)$, analytic and single-valued in $|z| > 1$, satisfying the mixed boundary conditions:

$$\begin{aligned} &\mathrm{Re}\,[h(z)] = -Ts, && \text{on meniscus 1,}\\ &\mathrm{Im}\,[h(z)] = T - \Omega, && \text{on solid portions,}\\ &\mathrm{Re}\,[h(z)] = -Ts + c_2, && \text{on meniscus 2}\,. \end{aligned} \tag{4.25}$$

(b) Solution using conformal slit mappings

Borrowing ideas on the use of conformal slit mappings in solving mixed boundary value problems of this kind as originally proposed by Crowdy [9] (see also [14]), it is now posed that a parametric solution for $h(z)$ satisfying the boundary conditions (4.25) is given by:

$$z = Z(\zeta), \qquad h = H(\zeta) = \mathrm{i}(T - \Omega) - \mathrm{i}T(\log Z(\zeta) - \log R(\zeta)), \qquad c_2 = -T\pi, \tag{4.26}$$

where the parametric complex variable ζ takes values in the upper-half annulus $\{D_\zeta^+ : \rho < |\zeta| < 1, \mathrm{Im}[\zeta] \geq 0\}$ and

$$Z(\zeta) \equiv -\frac{\omega(\zeta,\overline{\alpha})\omega(\zeta,1/\overline{\alpha})}{\omega(\zeta,\alpha)\omega(\zeta,1/\alpha)}, \qquad R(\zeta) \equiv -\frac{\omega(\zeta,\overline{\alpha})\omega(\zeta,1/\alpha)}{\omega(\zeta,\alpha)\omega(\zeta,1/\overline{\alpha})}, \tag{4.27}$$

where,

$$\omega(\zeta,\alpha) = -\frac{\alpha}{C^2}P(\zeta/\alpha,\rho), \qquad C = \prod_{n=1}^{\infty}(1-\rho^{2n}) \tag{4.28}$$

with $\alpha = \mathrm{i}r$ for $\rho < r < 1$ and where

$$P(\zeta,\rho) = (1-\zeta)\hat{P}(\zeta,\rho) \qquad \hat{P}(\zeta,\rho) \equiv \prod_{n=1}^{\infty}(1-\rho^{2n}\zeta)(1-\rho^{2n}/\zeta). \tag{4.29}$$

Downloaded from https://royalsocietypublishing.org/ on 28 October 2024

In (4.26), the principal branch of the complex logarithm is assumed with $\log X = \log|X| + \mathrm{i}\arg[X]$ with $-\pi < \arg[X] \le \pi$ so that the logarithm of a negative real quantity has imaginary part $\mathrm{i}\pi$.

The function $\omega(\zeta, \alpha)$ is the prime function for the concentric annulus $\{D_\zeta : \rho < |\zeta| < 1\}$ (see chapters 5 and 14 of Crowdy [14]) although its dependence on the parameter ρ is suppressed in the notation. An important feature is that the prime function $\omega(\zeta, \alpha)$ has a simple zero when $\zeta = \alpha$. On substitution of (4.28) into (4.27), it is also possible to write:

$$Z(\zeta) \equiv -\frac{P(\zeta/\overline{\alpha}, \rho)P(\zeta\overline{\alpha}, \rho)}{P(\zeta/\alpha, \rho)P(\zeta\alpha, \rho)}, \qquad R(\zeta) \equiv -\frac{P(\zeta/\overline{\alpha}, \rho)P(\zeta\alpha, \rho)}{P(\zeta/\alpha, \rho)P(\zeta\overline{\alpha}, \rho)}, \tag{4.30}$$

which highlights the dependence of $Z(\zeta)$ and $R(\zeta)$ on ρ. The formulas (4.30) will be used in what follows. It is a straightforward exercise to show, directly from the infinite product representation (4.29), that $P(\zeta, \rho)$ satisfies the two functional relations:

$$P(1/\zeta, \rho) = -\zeta^{-1}P(\zeta, \rho), \qquad P(\rho^2\zeta, \rho) = -\zeta^{-1}P(\zeta, \rho). \tag{4.31}$$

The two functions (4.30) built using the prime function are, respectively, examples of an unbounded circular slit map and an unbounded radial slit map as described in Crowdy [9,14] and Crowdy & Marshall [30]. The properties (4.31) can be used to confirm that the colour-coded images of the boundary portions of the upper half annulus D_ζ^+ under these two mappings are as shown in figure 2. In particular, the upper-half unit circle, denoted by C_0^+, is taken to be the preimage of the blue meniscus centred at $z = 1$ and the upper-half circle $|\zeta| = \rho$, denoted by C_1^+, is the preimage of the red meniscus centred at $z = -1$. The two intervals on the real axis, $-1 < \zeta < -\rho$ and $\rho < \zeta < 1$, are taken to be the preimages of the two no-slip boundary portions of the cylinder. From these geometrical properties, it can be verified, using properties of the complex logarithm, that $h(z)$ as given in (4.26) satisfies all the boundary conditions (4.25).

To confirm this, first note that the point α inside D_ζ^+ is the preimage of $z = \infty$. While the conformal map $Z(\zeta)$ has the necessary simple pole at this point, it is a removable logarithmic singularity of $h(z)$, which means the latter function is analytic as $z \to \infty$, as required. The mapping function $Z(\zeta)$ satisfies the functional identity:

$$Z(-\overline{\zeta}) = -\frac{P(-\overline{\zeta}/\overline{\alpha}, \rho)P(-\overline{\zeta}\overline{\alpha}, \rho)}{P(-\overline{\zeta}/\alpha, \rho)P(-\overline{\zeta}\alpha, \rho)} = -\frac{P(\overline{\zeta}/\alpha, \rho)P(\overline{\zeta}\alpha, \rho)}{P(\overline{\zeta}/\overline{\alpha}, \rho)P(\overline{\zeta}\overline{\alpha}, \rho)} = \overline{Z(\zeta)}, \tag{4.32}$$

which reveals that the images of any point ζ and that of $-\overline{\zeta}$ (the reflection of ζ in the imaginary ζ axis) are complex conjugates of each other in the z plane. This symmetry has two consequences. First, since C_0^+ and C_1^+ are taken to be the preimages of the two menisci, then the preimages of their centres are at $\zeta = \mathrm{i}, \mathrm{i}\rho$. Indeed, it can be verified that:

$$Z(\mathrm{i}) = 1, \qquad Z(\mathrm{i}\rho) = -1, \tag{4.33}$$

and the two menisci are reflectionally symmetric about the x axis. The symmetry (4.32) also confirms that the lengths of the images of the two segments of the real axis $-1 < \zeta < -\rho$ and $\rho < \zeta < 1$, which are taken to be the preimages of the two no-slip zones, must have the same circumferential lengths since the image of one is the reflection about the x axis of the other.

It is useful to remark here that to generalize the analysis to no-slip boundary portions of different lengths, it is simply necessary to allow the parameter α to move off the imaginary ζ axis but to remain in the upper-half annulus.

The conformal mapping in (4.30) depends on two unknown real parameters: r and ρ. For a given value of the angle Φ indicated in figure 2, the values of these two parameters are found by solving the two equations:

$$Z(1) = e^{\mathrm{i}\Phi}, \qquad Z(\rho) = e^{\mathrm{i}\Psi}, \qquad \Psi = \Phi + \pi\phi, \tag{4.34}$$

Downloaded from https://royalsocietypublishing.org/ on 28 October 2024

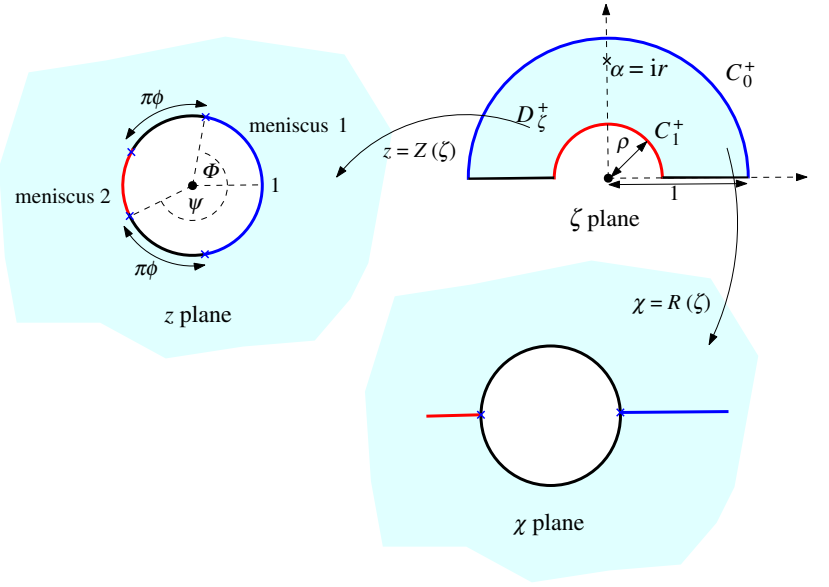


Figure 2. Conformal slit mappings, $Z(\zeta)$ and $R(\zeta)$, from an upper-half annulus $\{D_\zeta^+ : \rho < |\zeta| < 1, \mathrm{Im}[\zeta] \geq 0\}$ to an unbounded circular slit domain (in a complex z plane) and an unbounded radial slit domain (in a complex χ plane) [9,14,30]. Corresponding images under the respective maps are colour-coded. The point $\zeta = \alpha$ is the preimage of infinity in both cases.

where ϕ is the solid fraction so that $\pi\phi$ is the circumferential length of one of the solid portions; the angle Ψ is shown in figure 2. This is readily done using a nonlinear solver such as Newton's method.

Concerning the radial slit mapping, the two functional relations (4.31) can be used to show that the images of both C_0^+ and C_1^+ have constant argument. Indeed it can be verified using (4.30) that:

$$R(\mathrm{i}) = \left(\frac{P(-r,\rho)}{P(+r,\rho)}\right)^2, \qquad R(\mathrm{i}\rho) = -\left(\frac{P(-\rho r,\rho)}{P(+\rho r,\rho)}\right)^2, \tag{4.35}$$

revealing that the images under the radial slit mapping, in a complex χ plane say, of the points $\zeta = \mathrm{i}, \mathrm{i}\rho$ (corresponding to the centres of menisci 1 and 2) are, respectively, on the positive and negative real χ axis; indeed these correspond to the ends of the blue and red radial slits shown on the right in figure 2.

With these geometrical properties of the two conformal slit mappings $Z(\zeta)$ and $R(\zeta)$ established, it is easy to verify using the properties of the principal branch of the complex logarithm, that they satisfy:

$$\begin{aligned} &\mathrm{Re}\,[-\mathrm{i}T\log Z(\zeta)] = -Ts, && \text{on meniscus 1,}\\ &\mathrm{Im}\,[-\mathrm{i}T\log Z(\zeta)] = 0, && \text{on solid portions,}\\ &\mathrm{Re}\,[-\mathrm{i}T\log Z(\zeta)] = -Ts, && \text{on meniscus 2,} \end{aligned} \tag{4.36}$$

and

$$\begin{aligned} &\mathrm{Re}\,[\mathrm{i}T\log R(\zeta)] = 0, && \text{on meniscus 1,}\\ &\mathrm{Im}\,[\mathrm{i}T\log R(\zeta)] = 0, && \text{on solid portions,}\\ &\mathrm{Re}\,[\mathrm{i}T\log R(\zeta)] = -T\pi, && \text{on meniscus 2.} \end{aligned} \tag{4.37}$$

From these observations, the form of the required solution (4.26) satisfying (4.25) is now clear.

royalsocietypublishing.org/journal/rspa Proc. R. Soc. A 480: 20240149

Downloaded from https://royalsocietypublishing.org/ on 28 October 2024

With this parametric solution (4.26) at hand, it only remains to ensure that $h(z)$ has the far-field behaviour given in (4.15). It is shown in appendix A that this requires the condition:

$$\frac{\Omega}{T} = 1 - 2\log\left|\frac{P(+r^2,\rho)}{P(-r^2,\rho)}\right|, \tag{4.38}$$

which is the required mobility relation, and

$$U_c = 0, \qquad V_c = -T\left(\frac{P(-1,\rho)P(+r^2,\rho)}{\hat{P}(1,\rho)P(-r^2,\rho)}\right)\big(K(+r^2,\rho) - K(-r^2,\rho)\big), \tag{4.39}$$

where

$$K(\zeta,\rho) = \frac{\zeta}{P(\zeta,\rho)}\frac{\partial P(\zeta,\rho)}{\partial\zeta} = -\frac{\zeta}{1-\zeta} - \sum_{k=1}^{\infty}\frac{\rho^{2k}\zeta}{1-\rho^{2k}\zeta} + \sum_{k=1}^{\infty}\frac{\rho^{2k}/\zeta}{1-\rho^{2k}/\zeta}. \tag{4.40}$$

Formulas (4.39) give the velocity of the cylinder as an explicit function of T, ρ and r.

Although they did not consider the particular pattern of no-shear menisci and no-slip zones under consideration here, Siegel & Yariv [16] show that, if the distribution of ridges and menisci considered by them is symmetric about the real axis then $U_c = 0$ (in present notation). That observation is consistent with (4.39).

(c) $M = 1$ single meniscus limit $\rho \longrightarrow 0$

The problem of a single meniscus, the case $M = 1$, corresponds to the $\rho \to 0$ limit of the above analysis. The preimage ζ annulus reduces in this limit to the unit ζ disc. And, from (4.28), as $\rho \to 0$, the prime function for the concentric annulus $\rho < |\zeta| < 1$ reduces to the prime function for the unit disc [14], namely,

$$\omega(\zeta,\alpha) = \zeta - \alpha. \tag{4.41}$$

As explained in detail in Crowdy [14], with this modified definition of the prime function $\omega(\zeta,\alpha)$, the *same* formulas (4.27) continue to represent conformal slit mappings, this time from the upper unit disc $\{|\zeta| < 1, \mathrm{Im}[\zeta] > 0\}$ to the domains shown in figure 2 but now without the second circular and radial slits in the z and χ planes, respectively (and shown there in red). All the steps of the analysis §4b carry over to provide the solution:

$$z = Z(\zeta), \qquad h = H(\zeta) = \mathrm{i}(T-\Omega) - \mathrm{i}T\left(\log Z(\zeta) - \log R(\zeta)\right), \tag{4.42}$$

with $Z(\zeta)$ and $R(\zeta)$ again given by formulas (4.27), the only difference being that $\omega(\zeta,\alpha)$ is now defined by (4.41).

It is helpful here to preview a closely related result to come later. It will be shown in §5 that simply by defining yet more prime functions and using them in (4.42) and (4.27) that the solution to the $M > 2$ case is, in essence, immediate. The same formulas for the slit mappings, and the parametric representation of h, still pertain and only the definition of the relevant prime function changes. This underlines the fundamental theoretical importance of the prime function and conformal slit mappings built from them [14,28].

From (4.29) it also follows that, as $\rho \to 0$,

$$P(\zeta,\rho) \to 1-\zeta, \qquad K(\zeta,\rho) \to \frac{\zeta}{\zeta-1}. \tag{4.43}$$

Hence, in this limit, the mobility relation (4.38) becomes:

$$\frac{\Omega}{T} = 1 - 2\log\left(\frac{1-r^2}{1+r^2}\right). \tag{4.44}$$

Downloaded from https://royalsocietypublishing.org/ on 28 October 2024

Meniscus 1, the image of $|\zeta| = 1$, spans the particle circumference between $e^{-i\Phi}$ and $e^{+i\Phi}$ where $\Phi > 0$ so:

$$Z(1) = e^{i\Phi} = -\frac{(1-1/\overline{\alpha})(1-\overline{\alpha})}{(1-1/\alpha)(1-\alpha)} = \left(\frac{1-\overline{\alpha}}{1-\alpha}\right)^2. \tag{4.45}$$

On taking a square root, and choosing the minus sign to meet the requirement that $\rho < r < 1$, it is found that:

$$r = \tan(\Phi/4). \tag{4.46}$$

Expression (4.44) can then be written as:

$$\frac{\Omega}{T} = 1 - 2\log\left(\frac{1-\tan^2(\Phi/4)}{1+\tan^2(\Phi/4)}\right) = 1 - 2\log\cos(\Phi/2), \tag{4.47}$$

after use of familiar trigonometric identities. Yariv & Siegel [15] give the mobility relation for this problem in terms of a parameter ϕ defined to be the solid fraction of the cylinder boundary so that, in this case,

$$\phi = \frac{2\pi - 2\Phi}{2\pi}, \qquad \text{or} \qquad \Phi = \pi - \pi\phi. \tag{4.48}$$

Formula (4.47), rewritten in terms of ϕ, is

$$\frac{\Omega}{T} = 1 - 2\log\sin(\pi\phi/2) = 1 + 2\log\operatorname{cosec}(\pi\phi/2), \tag{4.49}$$

which retrieves the single-slot result (1.1) of Yariv & Siegel [15] providing a check on this alternative derivation using conformal slit mappings. Note that in the limit $\phi \to 0$, corresponding to a completely stress-free cylinder, $\Omega \to \infty$ indicating a singular solution as might be expected given that there are no solid boundary portions to provide any resistance against the external torque in this limit. Philip [6] observes similar blow-up of the effective slip length associated with transverse shear flow over a periodic array of no-shear slots when the no-slip fraction tends to zero.

It can also be shown using (4.39) together with (4.43) that, as $\rho \to 0$,

$$V_c \to \frac{4Tr^2}{(1+r^2)^2} = \frac{4T\tan^2(\Phi/4)}{(1+\tan^2(\Phi/4))^2} = T\sin^2(\Phi/2) = T\cos^2(\pi\phi/2), \tag{4.50}$$

where (4.46) and (4.48) have been used. For a given T, V_c is just a function of ϕ, and vanishes as $\phi \to 1$ as expected since this corresponds to the case of a solid cylinder without any no-shear slots considered in §3.

It is worth mentioning that in this $M = 1$ case, the parametric form of the solution in terms of the parameter ζ in the upper-half unit disc simplifies to:

$$z = -\frac{(\zeta+\alpha)(\zeta+1/\alpha)}{(\zeta-\alpha)(\zeta-1/\alpha)}, \qquad h = 2iT\left(\log\sin\left(\frac{\pi\phi}{2}\right) - \log\left(\frac{1/\alpha+\zeta}{1/\alpha-\zeta}\right)\right). \tag{4.51}$$

After some algebra, it is possible to eliminate ζ in these parametric formulas to find an explicit representation of $h(z)$ given by:

$$h(z) = 2T\left(i\log\sin\left(\frac{\pi\phi}{2}\right) + \cos^{-1}\left(\frac{\cos\kappa(z)}{\sin(\pi\phi/2)}\right) - \kappa(z)\right), \qquad \kappa(z) = (i/2)\log z, \tag{4.52}$$

where an appropriate branch of $\cos^{-1}$ must be taken; such expressions are reminiscent of formulas given by Philip [6] in solving a range of other mixed boundary problems. As discussed previously by the author in Crowdy [9] (where some of Philip's solutions were derived in a new parametric representation using conformal slit mapping arguments akin to those used above), there are several advantages in retaining use of the parametric

Downloaded from https://royalsocietypublishing.org/ on 28 October 2024

representation (4.51). Among the most important is that the parametric formulas encode the expected square root singularities at the transition points between no-slip and no-shear in an intrinsic way. Another reason is that, for $M \geq 2$, it is usually not possible to eliminate the parameter ζ analytically in any case.

Siegel & Yariv [16] devised a numerical scheme to compute the $M = 1$ solution (for a fixed cylinder) in a modified situation where the angular velocity of the superhydrophobic cylinder is set to unity with the required external torque then computed from the solution. In fig. 2 of Siegel & Yariv [16] the surface velocity in the anticlockwise direction along the meniscus, denoted there by $v(\theta)$ where θ is the usual cylindrical polar angle around the cylinder boundary, is plotted as a function of $\theta - \theta_m$, where θ_m is the polar angle of the centre of the meniscus, for five different values of solid fraction ϕ. In present notation, with $\theta_m = 0$, this quantity is

$$v(\theta) = -U(-\theta). \tag{4.53}$$

On use of (4.11) and (4.52), it can be shown, after some algebra and recalling that $\Omega = 1$ in [16] with T determined by the mobility relation (4.49), that:

$$v(\theta) = 1 - \frac{2}{1 - 2\log\sin(\pi\phi/2)}\mathrm{Im}\left[\cos^{-1}\left(\frac{\cos(\theta/2)}{\sin(\pi\phi/2)}\right)\right]. \tag{4.54}$$

As another check on the analysis, figure 3 reproduces fig. 2 of Siegel & Yariv [16] using (4.54) to compute the slip velocity $v(\theta)$ as a function of θ. Furthermore, a graph of $v(0)$ as a function of solid fraction ϕ shows it to have a minimum at $\phi \approx 0.27$, which is consistent with the numerically determined value reported in Siegel & Yariv [16].

(d) Illustrative calculations

Suppose the solid fraction is chosen to be $\phi = 1/2$ so that the circumferential length of each no-slip region is $2\pi\phi/2 = \pi/2$, figure 4 shows graphs of Ω/T and V_c/T, calculated using (4.38) and (4.39), as functions of Φ. This means that Φ ranges between $0 \leq \Phi \leq \pi/2$: as $\Phi \to 0$ meniscus 1 (shown in blue in figure 2) disappears while as $\Phi \to \pi/2$ meniscus 2 (shown in red in figure 2) disappears. These graphs are computed by first solving (4.34) for r and ρ given a value of Φ (and $\phi = 1/2$) and using these values to find Ω and V_c from formulas (4.38) and (4.39).

Several checks are available in this case. When $\Phi = 0, \pi/2$ the two no-slip zones merge and one of the menisci disappears leaving a cylinder with a single meniscus and no-slip fraction equal to $\phi = 1/2$. The results of formulas (4.38) and (4.39) should therefore coincide with the result (1.1) for $N = 1$ and $\phi = 1/2$ as corroborated by open circles in figure 4. When $\Phi = \pi/4$ the two no-slip zones have the same size as the two menisci and the patterning on the cylinder has symmetries about both the x and y axes (and a twofold rotational symmetry). The value of Ω should then coincide with that given by (1.1) when $N = 2$ and $\phi = 1/2$, as corroborated by a cross in figure 4. Moreover, in this case, V_c should vanish, which is the case.

These new analytical solutions, for two non-equal menisci generally devoid of any rotational symmetry, can therefore be viewed as providing a continuous interpolating set between the rotationally symmetric $N = 1$ and $N = 2$ solutions, both with solid fraction $\phi = 1/2$.

5. Superhydrophobic cylinders with $M > 2$ menisci

Suppose now that the cylinder has M menisci in general position around the boundary punctuated by M no-slip zones. Figure 5 shows a typical superhydrophobic cylinder with $M = 3$ no-shear menisci between $M = 3$ solid boundary portions of equal circumferential length; again, the latter restriction is not necessary and can readily be lifted. The preceding analysis has solved this problem for $M = 2$ and the central role in that analysis of the prime function defined in

Downloaded from https://royalsocietypublishing.org/ on 28 October 2024

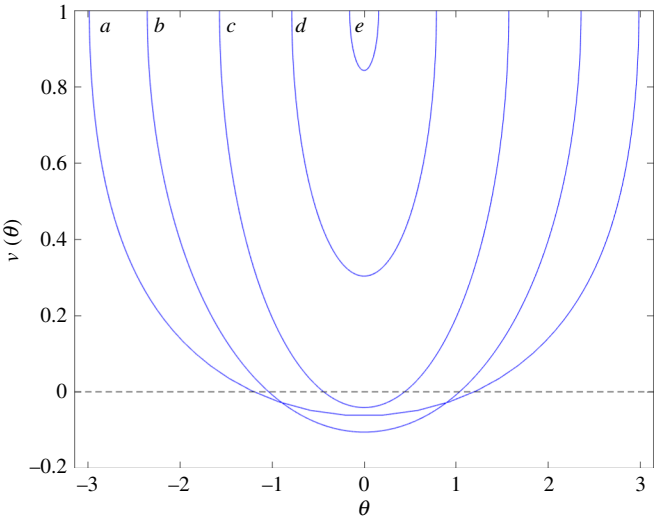


Figure 3. Reconstruction of fig. 2 of Siegel & Yariv [16] based on the new formula (4.54) for the slip velocity $\nu(\theta)$: graphs a, b, c, d and e correspond to solid fractions $\phi = 1/20$, 1/4,1/2,3/4 and 19/20, respectively.

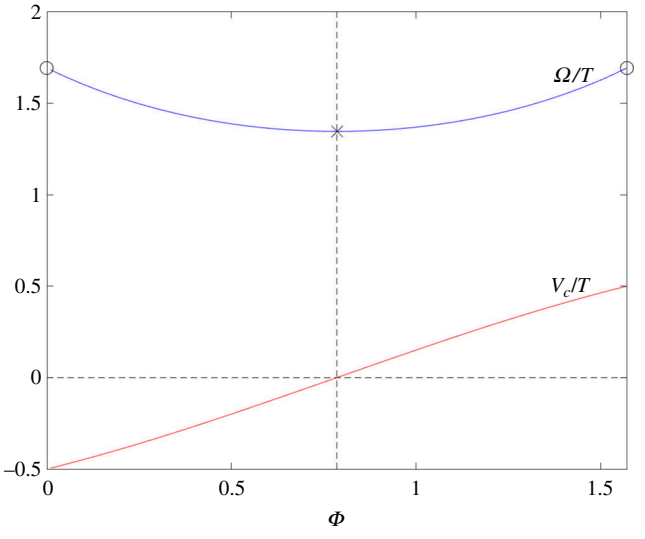


Figure 4. Graph of Ω/T and V_c/T as functions of Φ for $M = 2$ no-slip zones with solid fraction $\phi = 1/2$. The two open circles show the result (1.1) for $N = 1$ and $\phi = 1/2$; the cross shows the result (1.1) for $N = 2$ and $\phi = 1/2$. When $\Phi = \pi/4$ it is found that $V_c = 0$ as expected since the no-shear pattern now has twofold rotational symmetry.

(4.28), and associated with the concentric annulus relevant to that example, should be apparent. The concentric annulus is an example of a doubly connected circular domain, a domain whose boundaries are a union of circles. Prime functions can naturally be associated to any multiply connected circular domain, a mathematical fact whose theory has been expounded in detail in a recent monograph by the author [14]. Equipped with this mathematical machinery, the generalization of the $M = 2$ solution to any value of $M > 2$ is straightforward, a circumstance underscoring the theoretical importance of prime functions in applied mathematics [14,28]. The details for the $M = 3$ case will now be set out.

To find the torque-driven Stokes flow exterior to the superhydrophobic cylinder with $M = 3$ menisci and three equal-length solid portions shown in figure 5 a simple generalization of the

Downloaded from https://royalsocietypublishing.org/ on 28 October 2024

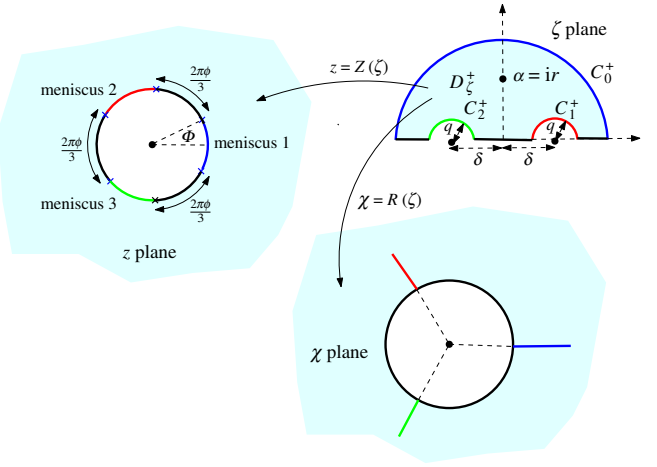


Figure 5. Conformal slit mappings, $Z(\zeta)$ and $R(\zeta)$, as given by (5.3) to an unbounded circular slit domain (in a complex z plane) and an unbounded radial slit domain (in a complex χ plane). The image in the z plane is the exterior of a circular superhydrophobic cylinder with $M = 3$ menisci punctuated by three no-slip zones of equal circumferential length. Corresponding images under the respective maps are colour-coded. The point $\zeta = \alpha$ is the preimage of infinity in both cases.

analysis of §4 leads to the need to solve for an analytic function $h(z)$, related to $f(z)$ via (4.14) as before, satisfying the mixed boundary conditions:

$$\begin{aligned} \mathrm{Re}\,[h(z)] &= -Ts, && \text{on meniscus 1,}\\ \mathrm{Im}\,[h(z)] &= T-\Omega, && \text{on solid portions,}\\ \mathrm{Re}\,[h(z)] &= -Ts+c_2, && \text{on meniscus 2,}\\ \mathrm{Re}\,[h(z)] &= -Ts+c_3, && \text{on meniscus 3,} \end{aligned} \tag{5.1}$$

where, as before, a constant of integration associated with meniscus 1 has been set to zero without loss of generality. There are now two other integration constants c_2 and c_3.

As already mentioned in §4c, a parametric solution for $h(z)$ using generalized conformal slit mappings is immediate given the prime function framework [14]. It is

$$z = Z(\zeta), \qquad h(z) = \mathrm{i}(T-\Omega) - \mathrm{i}T(\log Z(\zeta) - \log R(\zeta)), \tag{5.2}$$

where the parametric complex variable ζ takes values in the upper-half circular domain D_ζ^+ also shown in figure 5 and

$$Z(\zeta) \equiv -\frac{\omega(\zeta,\overline{\alpha})\omega(\zeta,1/\overline{\alpha})}{\omega(\zeta,\alpha)\omega(\zeta,1/\alpha)}, \qquad R(\zeta) \equiv -\frac{\omega(\zeta,\overline{\alpha})\omega(\zeta,1/\alpha)}{\omega(\zeta,\alpha)\omega(\zeta,1/\overline{\alpha})}, \tag{5.3}$$

with $\alpha = \mathrm{i}r$ for $0 < r < 1$. The only difference is that the function $\omega(.,.)$ must now be taken to be the prime function associated with a triply connected circular domain D_ζ comprising the unit disc $|\zeta| \le 1$ with two circular discs $|\zeta - \delta| < q$ and $|\zeta + \delta| < q$ excised; the unit circle will be denoted by C_0 and the two smaller circular boundaries $|\zeta - \delta| = q$ and $|\zeta + \delta| = q$ by C_1 and C_2, respectively. The domain D_ζ^+ is the upper-half of this circular domain D_ζ. The general theory of prime functions associated with circular domains such as D_ζ can be found in Crowdy [14] and appendix B surveys methods by which these special functions can be readily evaluated. An important feature of every prime function $\omega(\zeta,\alpha)$ is that is has a simple zero when $\zeta = \alpha$. It has other mathematical properties that ensure that formulas (5.3) continue to provide the requisite conformal slit mappings with the geometrical effect shown in figure 5 [29].

Downloaded from https://royalsocietypublishing.org/ on 28 October 2024

The upper half of the unit circle is denoted again by C_0^+ while the upper half of the circles $|\zeta-\delta|=q$ and $|\zeta+\delta|=q$ will be denoted by C_1^+ and C_2^+, respectively. For the superhydrophobic cylinder problem with three no-shear menisci, the images of the upper-half semi-circles C_0^+, C_1^+ and C_2^+ under the mapping $Z(\zeta)$ are taken to be the three no-shear menisci in the z plane, and the no-slip zones are the images of the three portions of the real ζ axis, shown in black in figure 5. The parameter α is taken to be located on the imaginary ζ axis, and the semi-circles C_1^+ and C_2^+ taken to have the same radius with centres symmetrically disposed about the ζ origin. Both of these provide necessary (but not sufficient) conditions for the three no-slip zones to have the same circumferential length.

In (5.2), the principal branch of the complex logarithm is assumed and it is easy to show that the constants c_2 and c_3 in (5.1) are related to the arguments of the radial slits shown schematically in figure 5. Formulas, in terms of the prime function, for these constants can be derived but they are not important for determining the mobility relation or cylinder speed so they are omitted here.

The mapping $Z(\zeta)$ now depends on three real parameters: q, δ and r. Suppose the solid fraction is chosen to be $\phi=1/2$ so that the circumferential length of each no-slip region is $2\pi\phi/3=\pi/3$, then q, δ and r must be chosen to satisfy the three conditions:

$$Z(1)=e^{\mathrm{i}\Phi}, \qquad Z(\delta+q)=e^{\mathrm{i}(\Phi+\pi/3)}, \qquad Z(\delta-q)=e^{5\pi\mathrm{i}/6}, \tag{5.4}$$

where the angle Φ is shown in figure 5. A nonlinear solver such as Newton's method applied to (5.4) leads easily to the requisite values of q, δ and r.

As before, the far-field asymptotics of the solution (5.2) as $|z|\to\infty$ provides the mobility relation and the speed of the cylinder. A straightforward adaptation of the analysis in appendix A leads to:

$$T-\Omega-2T\log\left|\frac{\omega(\alpha,1/\overline{\alpha})}{\omega(\alpha,1/\alpha)}\right|=0, \tag{5.5}$$

which, on rearrangement, gives the mobility relation:

$$\frac{\Omega}{T}=1-2\log\left|\frac{\omega(\alpha,1/\overline{\alpha})}{\omega(\alpha,1/\alpha)}\right|, \tag{5.6}$$

with the speed of the cylinder given, in complex form, by:

$$U_c+\mathrm{i}V_c=\frac{\mathrm{i}T}{\alpha}\left(\frac{\omega(\alpha,\overline{\alpha})\omega(\alpha,1/\overline{\alpha})}{\hat{\omega}(\alpha,\alpha)\omega(\alpha,1/\alpha)}\right)(K(\alpha,1/\overline{\alpha})-K(\alpha,1/\alpha)), \tag{5.7}$$

where

$$\hat{\omega}(\zeta,\alpha)=\frac{\omega(\zeta,\alpha)}{\zeta-\alpha}, \qquad K(\zeta,\alpha)\equiv\zeta\frac{\partial\log\omega(\zeta,\alpha)}{\partial\zeta}. \tag{5.8}$$

It is important to emphasize that although we have used the same function names $\omega(.,.)$ and $K(.,.)$ as in §4b, they refer now to different functions that are readily calculated following the discussion in appendix B. See also chapter 14 of Crowdy [14].

(a) Illustrative calculations

Figure 6 shows graphs of Ω/T and V_c/T as functions of Φ for three no-slip zones with solid fraction $\phi=1/2$ so that the circumferential length of each is $\pi/3$. This means that Φ takes values in the interval $0\le\Phi\le\pi/2$: when $\Phi\to 0$ meniscus 1 (shown in blue in figure 5) disappears while menisci 2 and 3 have the same circumferential length equal to $\pi/2$; when $\Phi=\pi/6$ all three menisci and the three solid portions have equal length $\pi/3$ and the cylinder has threefold

Downloaded from https://royalsocietypublishing.org/ on 28 October 2024

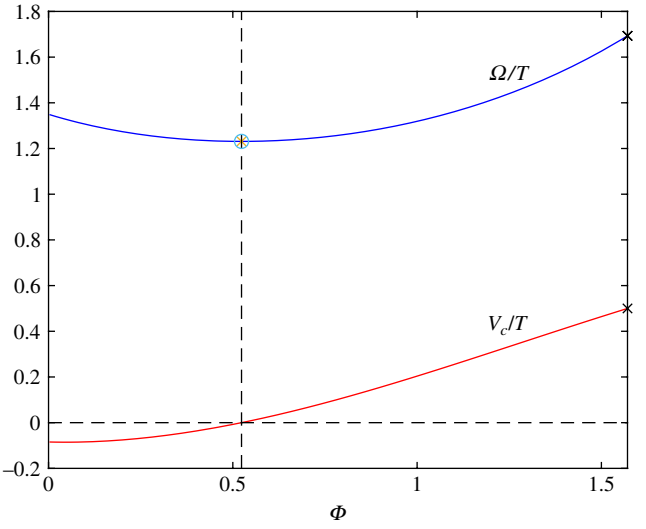


Figure 6. Graph of Ω/T and V_c/T as functions of Φ for three no-slip zones of fixed length $\pi/3$. The open circle shows the result (1.1) with $N = 3$ and $\phi = 1/2$, which is retrieved when $\Phi = \pi/6$. At that value, $V_c = 0$ as expected since the no-shear pattern now has threefold rotational symmetry. Crosses show the result from (1.1) and from (4.50) with $N = 1$ and $\phi = 1/2$, which are retrieved when $\Phi = \pi/2$.

rotational symmetry; when $\Phi \to \pi/2$ menisci 2 and 3 have disappeared and the problem reduces to the $M = 1$ solution with solid fraction $\phi = 1/2$. For each Φ, the relevant values of q, δ and r were found by solving (5.4) with those values then used in formulas (5.6) and (5.7) to compute Ω and V_c. It is found that $U_c = 0$ for all configurations. As a check on the calculation, the open circle in figure 6 shows the result (1.1) with $N = 3$ and $\phi = 1/2$ when $\Phi = \pi/6$: in this case, the superhydrophobic cylinder has threefold rotational symmetry and (1.1) applies. In this case, $V_c = 0$ as expected. When $\Phi = \pi/2$ all three solid portions have merged and the result (1.1) with $N = 1$ and $\phi = 1/2$ is retrieved.

When $\Phi \to 0$ so that meniscus 1 has disappeared leaving the two menisci 2 and 3, the results obtained in figure 6 will correspond to results given by an extension of the analysis for $M = 2$ in §4 to the case where the solid portions now have different lengths, equal to $\pi/3$ and $2\pi/3$. This generalization simply requires the point α to be off the imaginary axis and taken to be a more general point in the upper-half annulus D_ζ^+.

6. Swimming in circles

Having solved for the instantaneous flow around a superhydrophobic cylinder with a given no-shear surface pattern, the dynamical trajectory of such a particle can be found. Let $(X_c(t), Y_c(t))$ be the cylinder position at time t with initial condition $(X_c(0), Y_c(0)) = (0,0)$ and let $\theta(t)$ be the angle made with the positive real axis by the line joining the cylinder centre to the centre of meniscus 1 and with initial condition $\theta(0) = 0$. It is easy to show that the dynamics of the cylinder is described by the ordinary differential equations:

$$\frac{dX_c}{dt} = -V_c \sin\theta, \qquad \frac{dY_c}{dt} = V_c \cos\theta, \qquad \frac{d\theta}{dt} = \Omega, \tag{6.1}$$

where expressions for V_c and Ω have been found in this article as a function of the no-shear surface pattern. Since V_c and Ω are independent of time, it is easy to integrate the system (6.1)

Downloaded from https://royalsocietypublishing.org/ on 28 October 2024

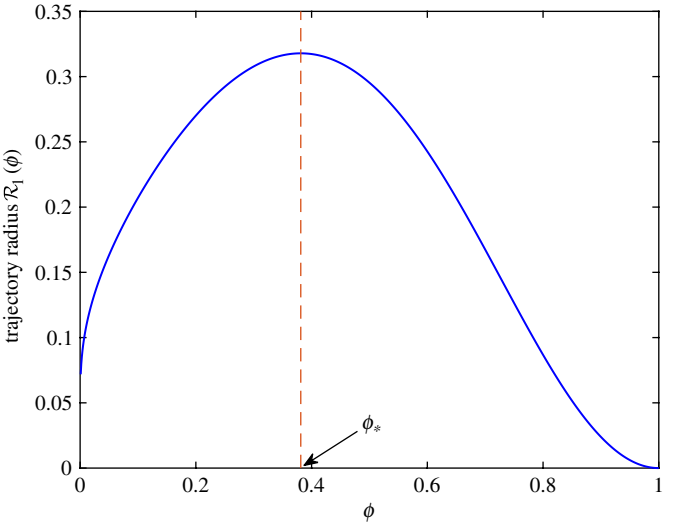


Figure 7. Radius $\mathcal{R}_1(\phi)$ of the circular trajectory of a swimming superhydrophobic cylinder with a single no-shear meniscus $M = 1$ as a function of the solid fraction ϕ for $0 < \phi \leq 1$. There is a maximum radius when the solid fraction is $\phi_* \approx 0.3813$, as given by formula (6.4).

subject to the specified initial conditions to find the complex location $Z_c(t) = X_c + \mathrm{i}Y_c(t)$ of the cylinder centre is:

$$Z_c(t) = \frac{V_c}{\Omega}(e^{\mathrm{i}\Omega t} - 1). \tag{6.2}$$

The trajectory of the cylinder is therefore a circle, centred at $(-V_c/\Omega, 0)$, with radius V_c/Ω. The angular velocity of the cylinder on this circular trajectory is Ω. Clearly, in the case where the no-shear patterning leads to $V_c = 0$, there is just rotation and no swimming in a circle.

From the analysis in §4c an explicit result is available for the case $M = 1$ of a single no-shear slot with solid fraction ϕ. Such a superhydrophobic cylinder swims in a circle with radius $\mathcal{R}_1(\phi)$ given by

$$\mathcal{R}_1(\phi) = \frac{\cos^2(\pi\phi/2)}{1 + 2\log\operatorname{cosec}(\pi\phi/2)}, \qquad 0 < \phi \leq 1, \tag{6.3}$$

which has made use of (4.50) and (4.49). A graph of $\mathcal{R}_1(\phi)$ as a function of solid fraction ϕ is shown in figure 7. An interesting feature is the existence of a maximum radius of this trajectory at a critical solid fraction ϕ_* found, after a calculus exercise, to be given explicitly by the formula:

$$\phi_* = \frac{2}{\pi}\sin^{-1}\left(-\frac{1}{W_{-1}(-1/e^2)}\right)^{1/2} \approx 0.3813, \tag{6.4}$$

where $W_{-1}(x)$ denotes the -1 branch of the Lambert W function [31]. The corresponding maximum radius is $\mathcal{R}_1(\phi_*) \approx 0.3178$.

From their numerical solution for this $M = 1$ case, Siegel & Yariv [16] observed a non-zero far-field speed, which they denoted by $\mathcal{A}_\phi$, for all $0 < \phi < 1$. In present notation, this should correspond to:

$$\mathcal{A}_\phi = -\mathcal{R}_1(\phi). \tag{6.5}$$

Downloaded from https://royalsocietypublishing.org/ on 28 October 2024

This is because in Siegel & Yariv [16], the angular velocity is set to be unity with T determined by (4.49), which, when substituted into (4.50) gives the correspondence (6.5); the negative sign appears because the cylinder is fixed in Siegel & Yariv [16]. It is easy to verify from the explicit expression (6.3) that $\mathcal{R}_1(1/2) \approx 0.295$ and $\mathcal{R}_1(3/4) \approx 0.126$, which are in agreement with the values of $-\mathcal{A}_{1/2}$ and $-\mathcal{A}_{3/4}$ reported in the caption of fig. 3 in Siegel & Yariv [16].

Consider now the trajectory of a swimming superhydrophobic cylinder with $M = 2$ no-shear menisci as shown in figure 2; these cylinders are characterized by the solid fraction ϕ and semi-angle Φ. Let the radius of a trajectory of such a cylinder be denoted by:

$$\mathcal{R}_2(\Phi, \phi) = \left| \frac{V_c}{\Omega} \right|, \tag{6.6}$$

where Ω and V_c are calculated from formulas (4.38) and (4.39). Figure 8 shows a graph of the radius $\mathcal{R}_2(\Phi, 1/2)$ as a function of Φ; this graph is easily produced using the data already presented in figure 4. As expected, the graph is symmetric about $\Phi = \pi/4$, at which value the cylinder has a twofold rotational symmetry and only rotates but does not swim in a circle.

Finally, consider the trajectory of a swimming superhydrophobic cylinder with $M = 3$ no-shear menisci as shown in figure 5; again, such cylinders are characterized by the solid fraction ϕ and semi-angle Φ. Let the radius of a trajectory of such a cylinder be denoted by:

$$\mathcal{R}_3(\Phi, \phi) = \left| \frac{V_c}{\Omega} \right|, \tag{6.7}$$

where formulas (5.6) and (5.7) are used to compute Ω and V_c. Figure 9 shows a graph of the radius $\mathcal{R}_3(\Phi, 1/2)$ as a function of Φ; this graph is easily produced using the data already presented in figure 6.

7. Superhydrophobic cylinders with N-fold rotational symmetry

Analytical solutions can also be found for flow exterior to an N-fold rotationally symmetric cylinder but where any representative sector has M menisci/no-slip zones. In what follows the N-fold rotationally symmetric problem shown in figure 10 (for $N = 4$) will be solved and, in doing so, the path to generalizing to any number M of menisci/no-slip zones per $2\pi/N$-sector should be clear.

It is important to bear in mind that the boundary value problem for the Stokes flow exterior to the cylinder is not conformally invariant meaning that care is needed when using conformal mapping to solve this generalized rotationally symmetric problem. By the assumed N-fold rotational symmetry, it is natural to introduce:

$$\mathcal{Z} = z^N, \tag{7.1}$$

a conformal mapping that sends a single $2\pi/N$ sector of the particle boundary to the same geometry already studied in the previous sections: figure 10 shows a schematic in the case $N = 4$ with $M = 2$ menisci per $2\pi/N$ sector. The choice of $g(z)$ is still given by

$$g(z) = -\mathrm{i}T\log z - \frac{f(z)}{z}, \tag{7.2}$$

and it is the analytic function:

$$H(\mathcal{Z}) \equiv \frac{2f(z)}{z}, \tag{7.3}$$

Downloaded from https://royalsocietypublishing.org/ on 28 October 2024

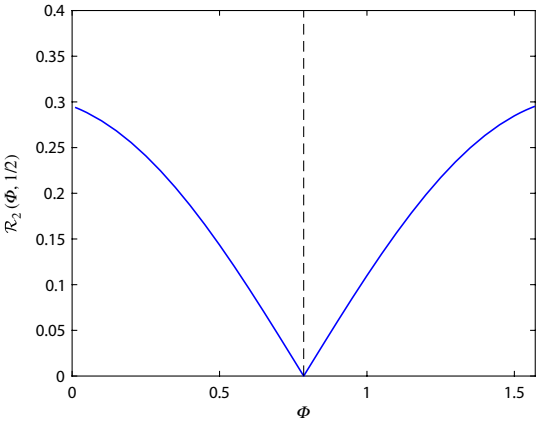


Figure 8. Radius $\mathcal{R}_2(\Phi, 1/2)$ of the circular trajectory of a swimming superhydrophobic cylinder with $M = 2$ no-shear menisci as a function of Φ as shown in figure 2. The graph is symmetric about $\Phi = \pi/4$ where the cylinder has a twofold rotational symmetry and only rotates but does not swim in a circle.

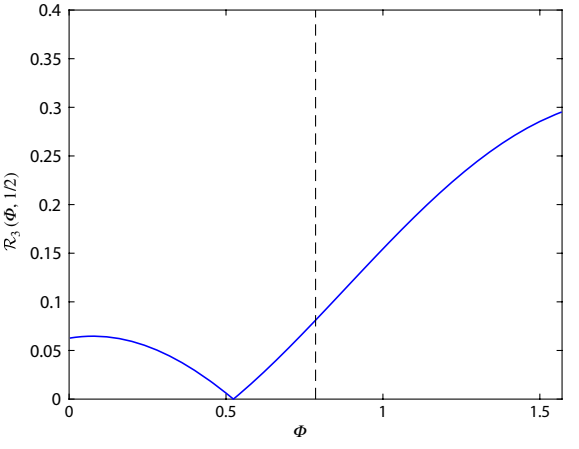


Figure 9. Radius $\mathcal{R}_3(\Phi, 1/2)$ of the circular trajectory of a swimming superhydrophobic cylinder with $M = 3$ no-shear menisci as a function of Φ as shown in figure 5. When $\Phi = \pi/6$ the cylinder has a threefold rotational symmetry and only rotates but does not swim in a circle.

that remains to be determined, albeit now as a function of $\mathcal{Z}$ and in the $\mathcal{Z}$ domain shown in figure 10. The boundary value problem for $H(\mathcal{Z})$ will now be formulated for the problem shown in figure 10.

First, the velocity condition on the solid boundary portions of the transformed cylinder in the $\mathcal{Z}$ domain remains the same, that is:

$$\mathrm{Im}\,[H(\mathcal{Z})] = T - \Omega\,. \tag{7.4}$$

The zero stress condition changes slightly, however. Since, by the chain rule,

$$z\frac{d}{dz} = N\mathcal{Z}\frac{d}{d\mathcal{Z}} \tag{7.5}$$

then condition (4.24) on the i-th meniscus in the $\mathcal{Z}$ plane becomes:

Downloaded from https://royalsocietypublishing.org/ on 28 October 2024

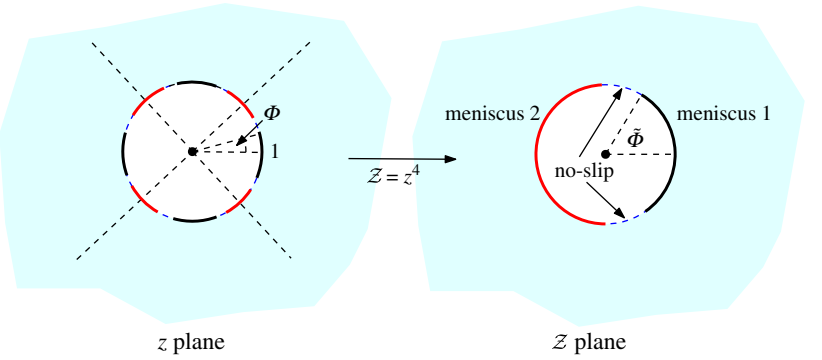


Figure 10. An N-fold rotationally superhydrophobic cylinder with $M = 2$ (generally different size) no-shear menisci in each sector of opening angle $2\pi/N$ (shown for $N = 4$). The transformation $\mathcal{Z} = z^N$ takes a principal sector to the domain already studied in §4.

$$\mathrm{Re}\,[H(\mathcal{Z})] = -\frac{TS}{N} + C_i, \tag{7.6}$$

where C_i are constants of integration and S is the arclength in the $\mathcal{Z}$ plane, i.e. $S = -\chi$ where $\mathcal{Z} = e^{\mathrm{i}\chi}$. The mixed boundary value problem for $H(\mathcal{Z})$, in the $\mathcal{Z}$ domain shown in figure 10, is now isomorphic to (but slightly different from) that already solved in §4b: find a function $H(\mathcal{Z})$ analytic and single-valued in $|\mathcal{Z}| > 1$ with the following mixed conditions on $|\mathcal{Z}| = 1$:

$$\begin{aligned} \mathrm{Re}\,[H(\mathcal{Z})] &= -\frac{TS}{N}, && \text{on meniscus 1,} \\ \mathrm{Im}\,[H(\mathcal{Z})] &= T - \Omega, && \text{on solid portions,} \\ \mathrm{Re}\,[H(\mathcal{Z})] &= -\frac{TS}{N} + c_2, && \text{on meniscus 2,} \end{aligned} \tag{7.7}$$

where the relevant menisci and no-slip portions are shown on the right in figure 10. Note that the angle $\tilde{\Phi}$ shown there is equal to $N\Phi$ where Φ is the angle in the principal sector indicated in the z-plane of figure 10. When $N = 1$, the boundary conditions (7.7) reduce to (4.25).

Simple alterations of the previous analysis given in §4 lead to the deduction that the parametric solution in terms of the variable ζ sitting in the upper half annulus $\rho < |\zeta| < 1, \mathrm{Im}[\zeta] \geq 0$ is:

$$\mathcal{Z} = Z(\zeta), \qquad H(\mathcal{Z}) = \mathrm{i}(T - \Omega) - \frac{\mathrm{i}T}{N}(\log Z(\zeta) - \log R(\zeta)). \tag{7.8}$$

As $|z| \to \infty$, so that $|\mathcal{Z}| \to \infty$ and $\zeta \to \alpha$, then

$$H(\mathcal{Z}) = \frac{2f(z)}{z} \sim h_0 + \frac{h_{-1}}{\mathcal{Z}} + \ldots, \tag{7.9}$$

where simple changes to the analysis in appendix A lead to:

$$\begin{aligned} h_0 &= \mathrm{i}(T - \Omega) - \frac{2\mathrm{i}T}{N}\log\left(\frac{P(+r^2, \rho)}{P(-r^2, \rho)}\right), \\ h_{-1} &= -\frac{2\mathrm{i}}{N}\left(\frac{P(-1, \rho)P(+r^2, \rho)}{\hat{P}(1, \rho)P(-r^2, \rho)}\right)\left(K(+r^2, \rho) - K(-r^2, \rho)\right). \end{aligned} \tag{7.10}$$

On comparison with (4.15), it is necessary that $\mathrm{Im}[h_0] = 0$ or

royalsocietypublishing.org/journal/rspa Proc. R. Soc. A 480: 20240149

Downloaded from https://royalsocietypublishing.org/ on 28 October 2024

$$T-\Omega-\frac{2T}{N}\log\left|\frac{P(+r^2,\rho)}{P(-r^2,\rho)}\right|=0, \tag{7.11}$$

which, on rearrangement, leads to:

$$\frac{\Omega}{T}=1-\frac{2}{N}\log\left|\frac{P(+r^2,\rho)}{P(-r^2,\rho)}\right|. \tag{7.12}$$

An important observation from (7.9) and (4.15) is that, for $N>1$, $U_c=V_c=0$ meaning that the particle does not translate, but only rotates. There is therefore no 'swimming in circles' as discussed in §6 unless $N=1$ and, even then, the surface patterning of M no-shear slots must be suitably asymmetric as quantified in previous sections.

A closely analogous $\rho\to 0$ analysis as carried out in §4c now leads to the modified result:

$$\frac{\Omega}{T}=1-\frac{2}{N}\log\cos(\tilde{\Phi}/2). \tag{7.13}$$

Since the no-slip fraction ϕ, taking account of all N solid portions, is

$$\phi=\frac{2\pi-2N\Phi}{2\pi}=\frac{2\pi-2\tilde{\Phi}}{2\pi},\qquad\text{or}\qquad\tilde{\Phi}=\pi-\pi\phi, \tag{7.14}$$

then (7.13) can be rewritten to retrieve (1.1), the mobility relation obtained, using quite different methods, by Yariv & Siegel [15] for an N-fold rotationally symmetric distribution of no-shear slots (with $M=1$ no-shear slot per $2\pi/N$ sector). Formula (7.12) generalizes this to $M=2$ no-shear slots per $2\pi/N$ sector and it should be clear from the analysis of this section how results for the case of $M>2$ no-shear slots per $2\pi/N$ sector can similarly be obtained by an analogous adaptation of the treatment given in §5.

A final remark is that an explicit solution is available for the N-fold rotationally symmetric problem with $M=1$ no-shear slot per $2\pi/N$ sector. It follows from the generalization explained in this section, combined with use of (4.52), that this problem has the solution:

$$h(z)=\frac{2T}{N}\left(\mathrm{i}\log\sin\left(\frac{\pi\phi}{2}\right)+\cos^{-1}\left(\frac{\cos\kappa(z)}{\sin(\pi\phi/2)}\right)-\kappa(z)\right),\qquad\kappa(z)=(\mathrm{i}/2)\log z^N. \tag{7.15}$$

8. Discussion

By using prime functions naturally associated with suitable multiply connected circular preimage domains to construct useful conformal slit mappings [14,28], analytical solutions for the torque-induced Stokes flow around a cylinder with any pattern of M no-shear menisci alternating with no-slip zones have been constructed. The flow around cylinders with N-fold rotationally symmetric patterning with each $2\pi/N$ sector containing M no-shear slots can also be found. Put together, this captures a wide range of superhydrophobic cylinder types.

Several cases have been solved explicitly, and other cases follow by straightforward generalization of the analysis in §§4 and 5. The reader will note how the parametric formulas (5.2) and (5.3) for $M=3$ menisci are formally identical to formulas (4.26) and (4.27) for just $M=2$ menisci, the only difference between them is that the prime function appropriate to the preimage circular domain must be used. This feature underscores not only the theoretical importance of the prime function as a mathematical tool, but the naturalness of the theoretical approach advanced herein. Indeed, the same formulas (4.26) and (4.27) also work for $M=1$ if the prime function is now defined by (4.41).

The approach is the radial-geometry analogue of a similar mathematical strategy, also based on conformal slit mappings, for finding transverse flows over periodic superhydrophobic surface advanced in Crowdy [9]. There are other closely related physical problems giving rise to mixed boundary value problems for Stokes flow that are also amenable to these techniques.

Downloaded from https://royalsocietypublishing.org/ on 28 October 2024

The problem of finding steady solutions involving steady 'stagnant caps' of insoluble surfactant on bubbles in an ambient Stokes flow is another where the author has shown that conformal slit mappings can play an enlightening role [32]; that work similarly retrieved, and extended, solutions found using alternative approaches based on Riemann–Hilbert methods [33]. For unsteady problems involving surfactant-loaded menisci numerical methods based on the use of conformal slit mappings also offer significant advantage [34].

Mixed boundary problems for Stokes flow also arise in soft matter problems involving active entities such as so-called Janus particles and the use of conformal slit mappings has been found of great utility there too [35,36]. The $M = 1$ superhydrophobic cylinder studied in explicit detail in §4c can be viewed as a two-faced Janus particle: it has one face that is solid, and another that differs in being a shear-free meniscus. The driving mechanism for motion here is the external torque and, in response to it, the untethered cylinders have been seen to swim in circles. This article has given a strategy for determining the radii of those circular trajectories, and the cylinder speed along them, analytically as functions of the no-shear pattern. A notable feature is that the trajectory radius for the $M = N = 1$ solution can be given explicitly as a function of the solid fraction by formula (6.3) and reveals that there is a maximum possible trajectory radius occurring at a critical solid fraction ϕ_*, also given by an explicit formula (6.4). The analysis here can be used to gain insight into the dynamical features of a wide range of superhydrophobic cylinder geometries.

The physical mechanism for providing the external torque on the superhydrophobic cylinder has not been discussed here. The cylinders fall within the broad class of propelled particles known as 'rotors' : this has become the general name given to particles that rotate in a fluid due to a torque that is either externally imposed, as is the case in this study, or internally generated [37]. A particle carrying a magnetic moment and sitting in a rotating magnetic field will experience a torque and such a system in a quasi-two-dimensional setting at a liquid–air interface has been studied both experimentally and theoretically in recent years [38–40]. It would be interesting to extend the present purely hydrodynamical study to incorporate additional multi-physics effects wherein the coupling, say, to an external magnetic field is also modelled.

Data accessibility. The calculations of this article can be repeated by the reader using freely downloadable MATLAB codes available at [40].

Declaration of AI use. I have not used AI-assisted technologies in creating this article.

Authors' contributions. D.G.C.: conceptualization, data curation, formal analysis, funding acquisition, investigation, methodology, project administration, writing—original draft, writing—review and editing.

Conflict of interest declaration. I declare I have no competing interests.

Funding. This work is partly funded by EPSRC Grant EP/V062298/1.

Appendix A. Far-field behaviour

To extract the far-field behaviour of $h(z)$ as $|z| \to \infty$, it is necessary to perform some local expansions of the parametric representation (4.26) around $\zeta = \alpha$, the preimage of the point at infinity. From (4.30) the following Laurent series is locally convergent in a neighbourhood of $\zeta = \alpha$:

$$z = Z(\zeta) = -\frac{P(\zeta/\overline{\alpha},\rho)P(\zeta\overline{\alpha},\rho)}{P(\zeta/\alpha,\rho)P(\zeta\alpha,\rho)} = -\frac{P(\zeta/\overline{\alpha},\rho)P(\zeta\overline{\alpha},\rho)}{(1-\zeta/\alpha)\hat{P}(\zeta/\alpha,\rho)P(\zeta\alpha,\rho)}$$
$$= \frac{\alpha P(\zeta/\overline{\alpha},\rho)P(\zeta\overline{\alpha},\rho)}{(\zeta-\alpha)\hat{P}(\zeta/\alpha,\rho)P(\zeta\alpha,\rho)} = \frac{A}{\zeta-\alpha} + B + \mathcal{O}(\zeta-\alpha), \tag{A 1}$$

where

Downloaded from https://royalsocietypublishing.org/ on 28 October 2024

$$A = \frac{\alpha P(-1,\rho)P(|\alpha|^2,\rho)}{\hat{P}(1,\rho)P(\alpha^2,\rho)}, \tag{A 2}$$

and where B is not important for present purposes. Similarly, a Taylor expansion of $H(\zeta)$ in a neighbourhood of $\zeta = \alpha$ leads to:

$$h(z) = \mathrm{i}(T-\Omega) - 2\mathrm{i}T\left[\log\left(\frac{P(|\alpha|^2,\rho)}{P(\alpha^2,\rho)}\right) + (\zeta-\alpha)\left(\frac{d}{d\zeta}\log\left(\frac{P(\zeta\overline{\alpha},\rho)}{P(\zeta\alpha,\rho)}\right)\right)_{\zeta=\alpha} + \mathcal{O}(\zeta-\alpha)^2\right]. \tag{A 3}$$

Since

$$\frac{d}{d\zeta}\log\left(\frac{P(\zeta\overline{\alpha},\rho)}{P(\zeta\alpha,\rho)}\right) = \frac{1}{\zeta}(K(\zeta\overline{\alpha},\rho) - K(\zeta\alpha,\rho)), \tag{A 4}$$

where $K(\zeta,\rho)$ is defined in (4.40), then:

$$h(z) = \mathrm{i}(T-\Omega) - 2\mathrm{i}T\left[\log\left(\frac{P(|\alpha|^2,\rho)}{P(\alpha^2,\rho)}\right) + \frac{A}{z}\frac{1}{\alpha}(K(|\alpha|^2,\rho) - K(\alpha^2,\rho)) + \mathcal{O}(1/z^2)\right], \tag{A 5}$$

where use has been made of (A 1). In order that $h(z)$ satisfies (4.15), it is necessary that the imaginary part of the leading order term in this expression vanishes, equivalently,

$$T - \Omega - 2T\log\left|\frac{P(+r^2,\rho)}{P(-r^2,\rho)}\right| = 0. \tag{A 6}$$

This can be rearranged to give the mobility relation (4.38). If this holds then the next term, at $\mathcal{O}(1/z)$, produces the result (4.39).

Appendix B. Calculation of the prime function

Analytical formulas for the Stokes flow solutions have been derived in terms of the prime function $\omega(.,.)$ of a multiply connected circular domain associated with a parametric variable ζ. Given such a circular domain, the most numerically efficient method to compute the associated prime function is to make use of freely available MATLAB codes [14,41]. These codes are based on a numerical algorithm described in detail in Crowdy & Marshall [42] and which extends an earlier algorithm proposed by Crowdy & Marshall [43].

For a triply connected domain such as that used in §5, however, it is also known (see chapter 14 of Crowdy [14]) that the infinite product representation:

$$\omega(z,\zeta) = (z-\zeta)\prod_{\Theta\in\Theta''}\frac{(\Theta(z)-\zeta)(\Theta(\zeta)-z)}{(\Theta(z)-z)(\Theta(\zeta)-\zeta)}, \tag{B 1}$$

is convergent; here, each function Θ lies in the set of Möbius maps Θ'' that denotes all elements of the free Schottky group generated by the basic Möbius maps:

$$\Theta_1(\zeta) \equiv \delta + \frac{q^2\zeta}{1-\delta\overline{\zeta}}, \qquad \Theta_2(\zeta) \equiv -\delta + \frac{q^2\zeta}{1+\delta\overline{\zeta}}, \tag{B 2}$$

except for the identity and excluding all inverses [14,43]. For numerical purposes of evaluation, it is necessary to truncate this product, and the natural way to do so is to include all Möbius maps up to a chosen level: see [14,43] for more details. Use of this infinite product is feasible for most superhydrophobic cylinder geometries, but maintaining a required degree of accuracy requires truncation at increasingly high levels as the radii of C_1 and C_2 get larger; then convergence of the product can become unacceptably slow. In such cases, use of the MATLAB code from [40] is preferred and advised.

Downloaded from https://royalsocietypublishing.org/ on 28 October 2024

References

1. Ou J, Rothstein JP. 2005 Direct velocity measurements of the flow past drag-reducing ultrahydrophobic surfaces. *Phys. Fluids* **17**, 103606. (doi:10.1063/1.2109867)
2. Rothstein JP. 2010 Slip on superhydrophobic surfaces. *Annu. Rev. Fluid Mech.* **42**, 89–109. (doi:10.1146/annurev-fluid-121108-145558)
3. Muralidhar P, Ferrer N, Daniello R, Rothstein JP. 2011 Influence of slip on the flow past superhydrophobic circular cylinders. *J. Fluid Mech.* **680**, 459–476. (doi:10.1017/jfm.2011.172)
4. Schnitzer O, Yariv E. 2019 Stokes resistance of a solid cylinder near a superhydrophobic surface. Part 1. Grooves perpendicular to cylinder axis. *J. Fluid Mech.* **868**, 212–243. (doi:10.1017/jfm.2019.177)
5. Lauga E, Stone HA. 2003 Effective slip in pressure-driven Stokes flow. *J. Fluid Mech.* **489**, 55–77. (doi:10.1017/S0022112003004695)
6. Philip JR. 1972 Flows satisfying mixed no-slip and no-shear conditions. *J. Appl. Math. Phys.* **23**, 353–372. (doi:10.1007/BF01595477)
7. Ya Moizhes B. 1975 Averaged electrostatic boundary conditions for metallic meshes. *Zh. Tekh. Fiz.* **25**, 167–176.
8. Veziroğlu T, Chandra S. 1968 *Thermal conductance of two-dimensional constrictions*. Miami, USA: University of Miami.
9. Crowdy D. 2011 Frictional slip lengths for unidirectional superhydrophobic grooved surfaces. *Phys. Fluids* **23**. (doi:10.1063/1.3605575)
10. Crowdy DG. 2010 Slip length for longitudinal shear flow over a dilute periodic mattress of protruding bubbles. *Phys. Fluids* **22**, 121703. (doi:10.1063/1.3531683)
11. Crowdy DG. 2016 Analytical formulae for longitudinal slip lengths over unidirectional superhydrophobic surfaces with curved menisci. *J. Fluid Mech.* **791**. (doi:10.1017/jfm.2016.88)
12. Crowdy DG. 2021 Superhydrophobic annular pipes: a theoretical study. *J. Fluid Mech.* **906**, A15. (doi:10.1017/jfm.2020.795)
13. Crowdy DG. 2021 Slip length formulas for longitudinal shear flow over a superhydrophobic grating with partially filled cavities. *J. Fluid Mech.* **925**, R2. (doi:10.1017/jfm.2021.709)
14. Crowdy DG. 2020 Solving problems in multiply connected domains. In *CBMS-NSF regional conference series in applied mathematics*. Philadelphia, PA: Society for Industrial and Applied Mathematics. (doi:10.1137/1.9781611976151). See https://epubs.siam.org/doi/book/10.1137/1.9781611976151.
15. Yariv E, Siegel M. 2019 Rotation of a superhydrophobic cylinder in a viscous liquid. *J. Fluid Mech.* **880**, R4. (doi:10.1017/jfm.2019.776)
16. Siegel M, Yariv E. 2023 Jeffery's paradox for the rotation of a single `stick–slip' cylinder, mech. *Res. Commun.* **131**, 104154. (doi:10.1016/j.mechrescom.2023.104154)
17. Purcell EM. 1977 Life at low Reynolds number. *Am. J. Phys.* **45**, 3–11. (doi:10.1119/1.10903)
18. Driscoll M, Delmotte B. 2019 Leveraging collective effects in externally driven colloidal suspensions: experiments and simulations. *Curr. Opin. Colloid Interface Sci.* **40**, 42–57. (doi:10.1016/j.cocis.2018.10.002)
19. Snezhko A. 2016 Complex collective dynamics of active torque-driven colloids at interfaces. *Curr. Opin. Colloid Interface Sci.* **21**, 65–75. (doi:10.1016/j.cocis.2015.11.010)
20. Lushi E, Vlahovska PM. 2015 Periodic and chaotic orbits of plane-confined micro-rotors in creeping flows. *J. Nonlinear Sci.* **25**, 1111–1123. (doi:10.1007/s00332-015-9254-9)
21. Driscoll M, Delmotte B, Youssef M, Sacanna S, Donev A, Chaikin P. 2017 Unstable fronts and motile structures formed by microrollers. *Nat. Phys.* **13**, 375–379. (doi:10.1038/nphys3970)
22. Delmotte B. 2019 Hydrodynamically bound states of a pair of microrollers: a dynamical system insight. *Phys. Rev. Fluids* **4**, 044302. (doi:10.1103/PhysRevFluids.4.044302)
23. Martínez-Pedrero F, Tierno P. 2018 Advances in colloidal manipulation and transport via hydrodynamic interactions. *J. Colloid Interface Sci.* **519**, 296–311. (doi:10.1016/j.jcis.2018.02.062)
24. Lauga E. 2016 Bacterial hydrodynamics. *Annu. Rev. Fluid Mech.* **48**, 105–130. (doi:10.1146/annurev-fluid-122414-034606)

25. Zöttl A, Stark H. 2016 Emergent behavior in active colloids. *J. Phys. Condens. Matter* **28**, 253001. (doi:10.1088/0953-8984/28/25/253001)
26. Kim S, Karrila SJ. 2005 *Microhydrodynamics*. New York, NY: Dover Publications.
27. Leal G. 2012 *Advanced transport phenomena*. Cambridge, UK: Cambridge University Press.
28. Crowdy DG. 2012 Conformal slit maps in applied mathematics. *ANZIAM J.* **53**, 171–189. (doi:10.1017/S1446181112000119)
29. Crowdy DG. 2020 Collective viscous propulsion of a two-dimensional flotilla of Marangoni boats. *Phys. Rev. Fluids* **5**, 124004. (doi:10.1103/PhysRevFluids.5.124004)
30. Crowdy DG, Marshall JS. 2006 Conformal mappings between canonical multiply connected domains. *Comput. Methods Funct. Theory* **6**, 59–76. (doi:10.1007/BF03321118)
31. Corless RM, Gonnet GH, Hare DEG, Jeffrey DJ, Knuth DE. 1996 On the Lambert W function. *Adv. Comput. Math.* **5**, 329–359. (doi:10.1007/BF02124750)
32. Siegel M. 1999 Influence of surfactant on rounded and pointed bubbles in two-dimensional Stokes flow. *SIAM J. Appl. Math.* **59**, 1998–2027. (doi:10.1137/S0036139997327435)
33. Fily Y, Baskaran A, Marchetti MC. 2012 Cooperative self-propulsion of active and passive rotors. *Soft Matter* **8**, 3002. (doi:10.1039/c2sm06952k)
34. Mayer MD, Crowdy DG. 2022 Superhydrophobic surface immobilisation by insoluble surfactant. *J. Fluid Mech.* **949**. (doi:10.1017/jfm.2022.677)
35. Crowdy DG. 2013 Wall effects on self-diffusiophoretic Janus particles: a theoretical study. *J. Fluid Mech.* **735**, 473–498. (doi:10.1017/jfm.2013.510)
36. Crowdy DG. 2013 Exact solutions for cylindrical 'slip–stick' Janus swimmers in Stokes flow. *J. Fluid Mech.* **719**. (doi:10.1017/jfm.2013.47)
37. Grzybowski BA, Stone HA, Whitesides GM. 2000 Dynamic self-assembly of magnetized, millimetre-sized objects rotating at a liquid–air interface. *Nature* **405**, 1033–1036. (doi:10.1038/35016528)
38. Grzybowski BA, Jiang X, Stone HA, Whitesides GM. 2001 Dynamic, self-assembled aggregates of magnetized, millimeter-sized objects rotating at the liquid-air interface: macroscopic, two-dimensional classical artificial atoms and molecules. *Phys. Rev. E* **64**. (doi:10.1103/PhysRevE.64.011603)
39. Climent E, Yeo K, Maxey MR, Karniadakis GE. 2007 Dynamic self-assembly of spinning particles. *J. Fluids Eng.* **129**, 379–387. (doi:10.1115/1.2436587)
40. Open source MATLAB codes. See https://github.com/ACCA-Imperial.
41. Crowdy DG, Kropf EH, Green CC, Nasser MMS. 2016 The Schottky–Klein prime function: a theoretical and computational tool for applications. *IMA J. Appl. Math.* **81**, 589–628. (doi:10.1093/imamat/hxw028)
42. Crowdy DG, Marshall JS. 2007 Computing the Schottky-Klein prime function on the Schottky double of planar domains. *Comput. Methods Funct. Theory* **7**, 293–308. (doi:10.1007/BF03321646)
43. Crowdy DG. 2013 Surfactant-induced stagnant zones in the Jeong-Moffatt free surface Stokes flow problem. *Phys. Fluids* **25**, 092104. (doi:10.1063/1.4821137)

Downloaded from https://royalsocietypublishing.org/ on 28 October 2024